Wide field-of-view all-reflective objectives designed for multispectral image acquisition in photogrammetric applications

Kristof Seidl[a,b], Katja Richter[a], Jens Knobbe[b], Hans-Gerd Maas*[a]
[a] Technische Universität Dresden, Institute of Photogrammetry and Remote Sensing, Helmholtzstr. 10, DE-01062 Dresden
[b] Fraunhofer Institute for Photonic Microsystems, Maria-Reiche-Str. 2, D-01109 Dresden

ABSTRACT

In many aerial and close-range photogrammetric applications, the near infrared (NIR) spectral range is required in addition to the visible (VIS) spectral range. Currently, most photogrammetric systems use particularly optimized camera systems for each spectral band. Using separate cameras or lenses can introduce parallaxes and time-delays between the acquired images, and thus complicate the data fusion process. Furthermore, it adds additional weight to the entire system. With an image acquisition through a single objective, the complexity of the data fusion and the weight can be significantly reduced. However, to be able to only use one objective for different spectral bands, the optical system has to be free of chromatic aberrations. For photogrammetric applications, a wide field-of-view and a high resolution are additional requirements.

Therefore, we will present a design and an adapted photogrammetric calibration method of an all-reflective unobscured optical system optimized for full-frame imaging sensors. All-reflective unobscured optical systems may also be a very efficient imaging tool in combination with unmanned aerial vehicles (UAVs). Due to the limited payload capacity, many currently available UAVs can only be used with one spectrally limited camera system at the same time. With miniaturized all-reflective camera systems, the image data could be acquired in the visible and e.g. the NIR spectral range simultaneously.

Keywords: all-reflective unobscured objective, photogrammetric calibration, unmanned aerial vehicle (UAV)

1. INTRODUCTION

In the past, we developed an all-reflective unobscured objective with four mirrors, where the focal length could be changed if the curvatures of two mirrors are variable [1]. Figure 1 show the optical design of this system for three different focal lengths. In an optical-power zoom (OPZ) objective at least two elements or groups have to be variable. In case of our all-reflective unobscured OPZ objective, the first and last mirrors are the variable elements.

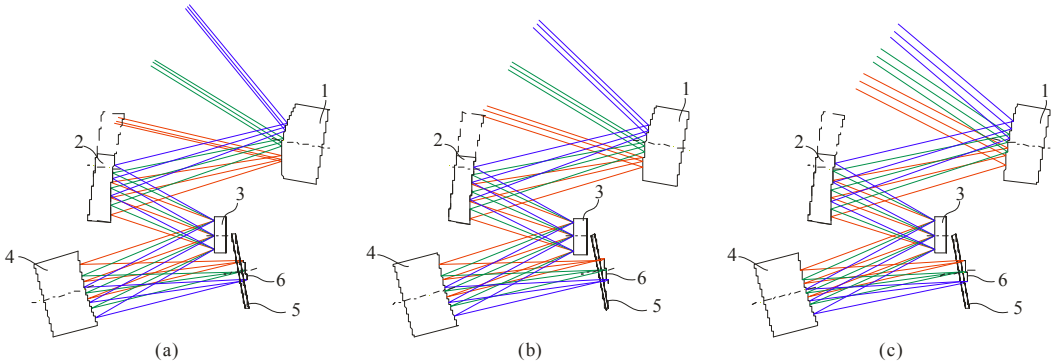

Figure 1. Final design of the all-reflective unobscured objective with curvature-variable mirrors – (a) f' = 5.2 mm, (b) f' = 7.8 mm, (c) f' = 15.6 mm; 1 first deformable mirror (DM), 2 off-axis biconic concave mirror, 3 biconic convex mirror (acts as aperture stop), 4 second DM, 5 cover glass, 6 image sensor

* hans-gerd.maas@tu-dresden.de

For a mirror zoom objective, which uses a 1/3”-image sensor and provides a field-of-view between 60° and 20°, variable mirrors with a diameter of at least 12 mm and absolute radii between 17.8 mm and 51.7 mm are required. Deformable mirrors with such specifications are not available today, and hence further development of elastic materials and shapes is necessary to realize this type of an all-reflective objective. Nevertheless, to show the optical performance of our approach, we built up a demonstration system consisting of three opto-mechanically identical setups for three different focal lengths (see Figure 2).

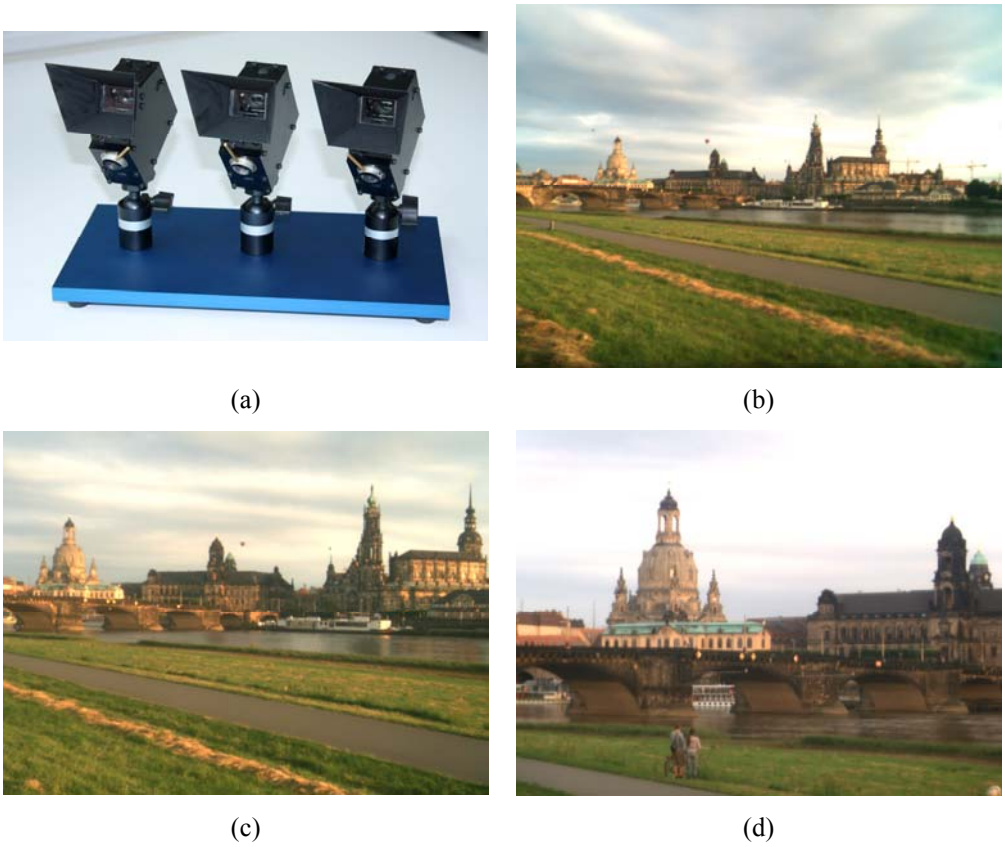

(a) (b)

(c) (d)

Figure 2. demonstration system (a) and images taken with different focal lengths (b) f' = 5.2 mm, (c) f' = 7.8 mm, (d) f' = 15.6 mm.

The three focal lengths of the system were realized by using different solid mirrors manufactured by ultra-precisions turning and milling technologies. Successively, acquiring images from all three cameras the changing field-of-view can be demonstrated.

Being free of chromatic aberrations, all-reflective unobscured objectives have a very high potential even without the zooming functionality. While the deformable mirrors with the specifications required can not be provided, we will concentrate us to enhance the so called “Schiefspiegler”-approach to a multispectral imaging tool with a fixed focal length. Especially in aerial and close-range photogrammetric applications, where multispectral images should be acquired simultaneously from the same position, the use of “Schiefspiegler” objectives will have considerable advantages. Examples for such applications are the restoration of historical buildings [2], agriculture purposes [4], or security applications [5].

Today, camera systems have specially optimized lenses for their spectral range. Thus, the images are either acquired one after another from the same position or simultaneously with a parallax. Both methods make the preparation and evaluation of the data as well as the subsequent determination of the 3D object coordinates highly complex. Image data acquisition through one objective can reduce the complexity of the data fusion process. However, in order to only use one objective for different spectral bands, the optical system has to be free of chromatic aberrations. Furthermore, the

objective needs a large back focal length to split the beam path for two different spectral ranges before the light is reaching the image sensors. For close range photogrammetric applications, where 3D object coordinates should be extracted from large objects with a high accuracy, a wide field-of-view and a very high image quality are additional requirements. To fulfill these requirements without making the whole system too complex, a retrofocus type all-reflective unobscured objective with a fixed focal length should be preferred. The aberrations of a four-mirror unobscured objective like coma and astigmatism can be more reduced for an objective with a fixed focal length than for the mirror zoom objective presented above. The image quality could be further optimized by using a high resolution full-frame image sensor with a large pixel size instead of a 1/3" image sensor. For close range photogrammetric applications, the size and weight of the camera system are not as crucial as for robotic applications or applications using unmanned aerial vehicles. Due to the limited payload capacity, many vehicles can nowadays only be used with one spectrally limited camera system at the same time. With miniaturized all-reflective camera systems, the image data can be acquired in the visible and e.g. the NIR spectral range simultaneously.

Following, we will present the designs of an all-reflective objective, particularly optimized for a full-frame image sensor, and of a monolithic objective with four mirror surfaces that is intended as imaging tool for robotics or in combination with an UAV.

Subsequently, we will show first results of a photogrammetric calibration method for the OPZ system to get an estimate of accuracy that can be reached for the determined 3D object coordinates.

2. OPTICAL DESIGN

2.1 Dual-band all-reflective unobscured objective for full-frame image sensors

The optical design for the full-frame all-reflective unobscured objective was scaled up from the OPZ design presented earlier. Because photogrammetric applications almost use objectives with a fixed focal length, the additional degrees of freedom can be used for a better aberration correction compared to the OPZ objective. The additional degrees of freedom comprise beside the fixed focal length also rotational unsymmetrical surfaces for all mirror surfaces. For splitting the light in the objective into two different optical paths according to the spectral ranges, a beam-splitter plate with a dichroic coating should be used. However, this plate causes coma and astigmatism for the ray bundles passing the plate, because they are divergent. The aberration can be minimized with a thin plate, which is tilted as little as possible. However, the minimum tilt angle is limited by the fact that no obscuration should occurred. In our case, the beam splitter plate has a thickness of 1.1 mm and is tilted by 33°. The residual coma and astigmatism can be further reduced with optimized aspheric mirror surfaces and a slightly tilted dome in front of the first mirror. Besides reducing coma and astigmatism, this dome also protects the whole objective against environmental influences. Due to the wide spectral range we strive for, the dome will be made of infrared grade fused silica, which has an applicable transparency up to 3.5 µm [6], and posses an antireflection coating, which is adapted to the addressed spectral range.

In Figure 3 a first optical and an opto-mechanical design of the full-frame dual band all-reflective unobscured objective as well as the MTF-plot are shown. The objective has a field-of-view of 27°x40°, which corresponds to a focal length $f' = 47$ mm. Furthermore, it has minimum f-number of $f/3.5$. Two precision linear stages, which have perpendicular axes, allow for the movement and thus for the accurate alignment of the two image sensors. For focusing the objective, the position of the sensor assembly can be changed with an additional linear stage. The sensor assembly comprises the two image sensors and the beam splitter plate.

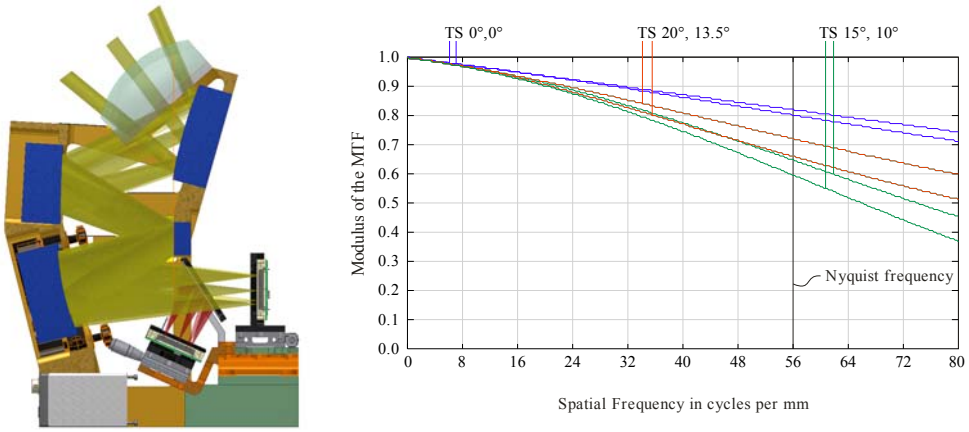

(a) (b)

Figure 3. (a) first design for a full-frame dual-band all-reflective unobscured objective with a full field-of-view of 27°x40° and *f* / 3.5; (b) MTF for the visual spectral range.

2.2 Monolithic objective with four mirror surfaces intended as imaging tool for robotics and UAVs

The experience we acquired during the design of the OPZ shows that the requirements of a multispectral imaging tool for robotics and UAVs are quite sophisticated. For the OPZ-demonstrators presented above, the opto-mechanical mounts for the mirrors need a lot of space and cause the major portion of the system weight. A camera system for a robot or a UAV, however, needs to be very compact and lightweight. It is well known that UAVs in particular have a very limited payload. The specified maximum payload capacity for the Falcon 8 from Ascending Technologies (see Figure 4), for example, is 500 g [8]. The smaller the payload the more flight time will be available. At the maximum payload, the Falcon 8 has a flight time between 16 min and 18 min [8].

The challenge for the design of a dual-band camera system for a UAV is to find a compromise between weight and stability to keep the narrow opto-mechanical tolerances. To address the two opposing properties, we choose a slightly different approach than we did for the OPZ or the full-frame unobscured objective.

Figure 4. Unmanned aerial vehicle (UAV) Ascending Technologies Falcon 8 with mounted OPZ demonstration system

To stint the heavy mounts of the mirrors, but simultaneously preserve the stability of the objective, the objective needs to be self-supporting. This can be, for instance, achieved with a monolithic matter, which has refractive and reflective surfaces similar to the design presented in [9].

Instead of having air between the reflective surfaces, the objective consists of a “single piece of machined or molded acrylic” [10]. However, the design presented in [10] has a field-of-view of 5° only. For the large field-of-view required for the intended applications, a four-mirror design is needed again. The major advantage that all-reflective objectives are free of chromatic aberrations, however, will be lost, when using refractive surfaces, too. With a deliberate arrangement of the two refractive surfaces, however, chromatic aberrations can almost be eliminated without an additional achromatization. If the center of the curvature of the first refractive surface, where the rays enter the monolithic material, coincides with the center of the entrance pupil, the refractive effect of the first surface will be marginal. Thus, the chromatic aberration caused by the surface could be minimized. The second refractive surface of the monolithic objective will be the exit surface. Due to the short distance between the exit surface and the image sensor, which will be a fraction of a millimeter only, the effect of chromatic aberration will be minimal. The exit surface would be a predestinated surface for cementing the image sensor assembly well-defined onto the monolithic objective. This could be either done with the help of a commonly used cover glass or through directly mounting the chip carrier without any glass.

The size of the image sensor will be the decisive factor for the size and weight of the whole camera system. For UAV applications a 1/3” or 1/2” image sensor could be a good compromise between weight and obtainable image quality. Figure 5 shows an example for the design of a dual-band monolithic objective with a 1/2” image sensor. The objective has a field-of-view of 27°x35°, which corresponds to a focal length f' = 10 mm. The minimum f-number is f/3.5. It was decided to use Zeonex® as the material for the monolithic objective. Zeonex® can be molded or ultra-precision machined and has an acceptable transparency in the visible and in the near infrared spectrum up to a wavelength of 2.2µm [9]. To separate the beam paths for both spectral ranges, an additional prism with a dichroic coating is needed. Together with one image sensor, the prism can be cemented onto the monolithic objective. Therewith, the arrangement does not cause different aberrations for the two beam paths as the beam splitter plate in the full-frame objective does.

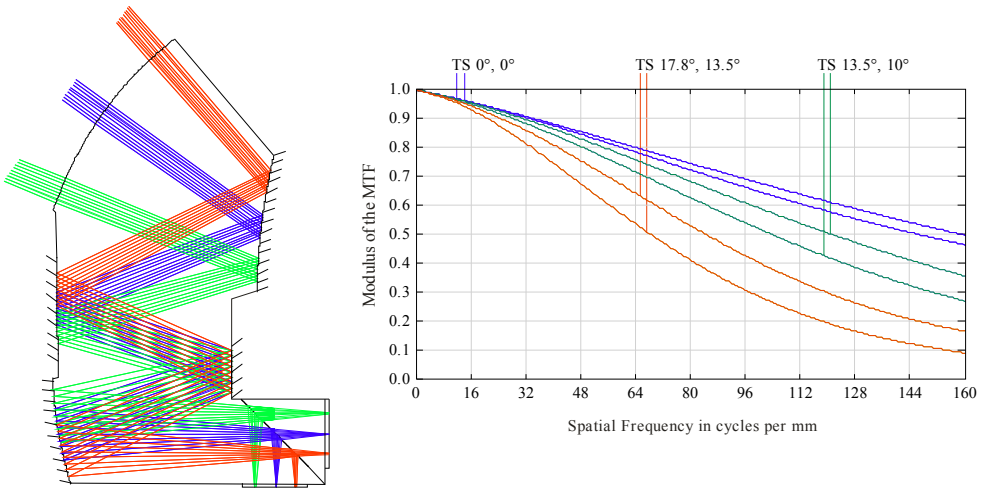

(a) (b)

Figure 5. (a) first design for a monolithic dual-band unobscured objective with a 1/2”-image sensor; full field-of-view of 27° x 35.5° and f/3.5; (b) MTF for the visual spectral range.

It is predicted that the monolithic solution would be three times lighter than one OPZ demonstration system including both image sensors. The weight of the objective in Figure 5 could be considerably less than 100 g at a size of approximately 50 mm x 30 mm x 30 mm.

Until the concept presented above can be realized, there are quite some problems to solve. The molding process seems to be a particularly difficult part. The material needs to be homogeneous, without bubbles or particles. Furthermore, the mirror surfaces have to keep extreme narrow tolerances. For a first demonstration system the ultra-precision milling and turning technology should be preferred.

3. PHOTOGRAMMETIC CALIBRATION

The designed objectives will achieve an image quality, which is adequate for most of the indented photogrammetric applications. Due to their similar optical design, the objectives will show similar distortion effects as the OPZ objective. Figure 6 shows the distorted images of the three different zooming positions of the OPZ setups. In [7] we presented a first method to correct the rotational unsymmetric distortion effects. The results of this correction can be seen in Figure 2. Following we will verify this model by photogrammetric calibration methods and introduce improved models. Later on, it is intended to use the improved calibration models for the full-frame all-reflective dual-band unobscured objective and the monolithic objective, too.

The main reason for the significant amount of distortion is the curvature of the primary mirror. The higher the curvature of the first mirror, the more distortion will be introduced into the system. Most notably is the distortion for the smallest focal length with the curved lines. The distortion of the images is non-rotational symmetric and, most of all, negative.

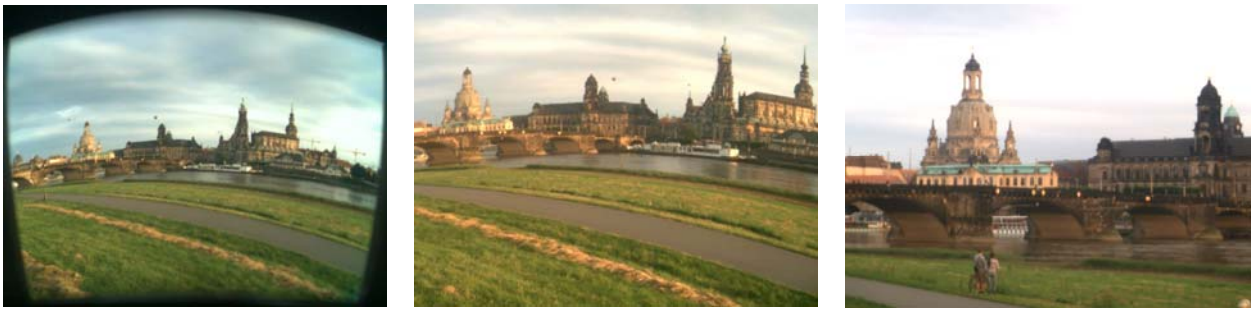

(a) (b) (c)

Figure 6. Distorted images taken with OPZ setups: (a) f '= 5.2 mm, (b) f '= 7.8 mm, and (c) f '= 15.6 mm.

To correct the distortion effects the undistorted position of each image point has to be calculated. Therefore, accurate distortion models and practicable calibration methods are needed. The coordinates x' and y' of distorted images can be estimated with

$$\begin{aligned} x' &= x + \Delta x \\ y' &= y + \Delta y \,, \end{aligned} \tag{1}$$

where x and y are the coordinates without distortion and Δx and Δy are the absolute deviations of the distorted image points from the undistorted ones.

In [7] we already presented a feasible distortion model. It includes the parameters R_1 and R_2 for radial-symmetric distortion, K and B for keystone and bowing distortion, S for shortening and stretching effects, and A_1 and A_2 for anamorphotism

$$\begin{aligned} x' &= x + xr^2\left(R_1 + R_2 r^2\right) + 2Kxy\left(R_1 + R_2 r^2\right) + A_1 x + A_2 x^3 \\ y' &= y + yr^2\left(R_1 + R_2 r^2\right) - Br^2\left(R_1 + R_2 r^2\right) + 2Sy^2\left(R_1 + R_2 r^2\right) + 3A_1 y - A_2 y^3 \end{aligned} \tag{2}$$

with $r = \sqrt{x^2 + y^2}$.

We obtained the parameters for eq. (2) from simulation data calculated by an optical design software. The resulting parameters for the wide-angle zoom position, the root mean square (RMS), and the maximum of the remaining distances between the real and the distorted image points are shown in Table 1.

Table 1. Optimized distortion parameters and residual deviation for the wide-angle zoom position

f/mm	R_1	R_2	*K*	*B*	*S*	A_1	A_2	s_0 */mm*	*max/pixel*
5.17	-0.0176	3.11e-4	0.991	2.71	0.796	-6.87e-4	8.47e-4	0.0014	2.88

To verify the accuracy of our distortion model we compared the achieved results with photogrammetric calibration methods.

The goal of photogrammetric calibration is the determination of the interior orientation of a camera. Parameters used to characterize the interior orientation of a central perspective camera are the coordinates of the principal point, the principal distance, as well as parameters of the distortion model. In close range photogrammetry mathematical methods are used to determine unknown parameters via known image- and 3D coordinates of object points. With the help of a basic algorithm called spatial resection, it is possible to calculate the sought-after parameters on the basis of one image.

The distortion model, which was presented earlier, was implemented into a spatial resection. The resulting parameters and quality criteria are presented in Table 2.

Table 2. Optimized distortion parameters and residual deviation determined by spatial resection

f/mm	R_1	R_2	*K*	*B*	*S*	A_1	A_2	s_0 */mm*	*max/pixel*
5.17	-0.0124	2.00e-4	1.341	4.04	1.554	-0.042	-0.003	0.0282	6.28

When comparing the corresponding values with each other, significant differences for most of the estimated parameters are found. The reason for this deviation is that geometrical model and physical reality only roughly correspond with each other. Hence, the parameters obtained from the simulation data can solely be applied for the visual correction of distorted images. The residual distortion is not visible. In order to use the OPZ objective for measurement applications, it is necessary to estimate the parameters from real image data. Furthermore, the presented model needs to be improved with the help of photogrammetric methods. Coordinates of the principal point and the principal distance could be, for instance, included into the model. Subsequently, we will call the enhanced model “Seidl”. Moreover, tests with alternative sets of additional parameters should be conducted.

The basic mathematical principles of spatial resection apply to the model of a central perspective camera. Concerning the optical design, the OPZ does not correspond with this model. However, as an accurate geometric model can be more complex, we try to adapt the central perspective model to our objective. We are aware of the fact that the estimated parameters have no physical interpretability.

Generally, a set of additional parameters developed by Brown [11] is used to model the distortion of digital cameras. His model consists of three parameters for the radial symmetric distortion (R_1, R_2, R_3), two parameters for the tangential distortion (B_1, B_2), and two parameters for affinity and shear (C_1, C_2). Expectedly, it is not possible to use all interior orientation parameters for the OPZ. Some parameters have to be eliminated to achieve a convergence. With the remaining parameters, we could realize an accuracy of s_0 = 0.0445 mm. Figure 7 shows the residuals after the adjustment

and indicates that the chosen parameters are not able to correct all distortion effects. Consequently, additional parameters are necessary to optimize the modeling of distortion.

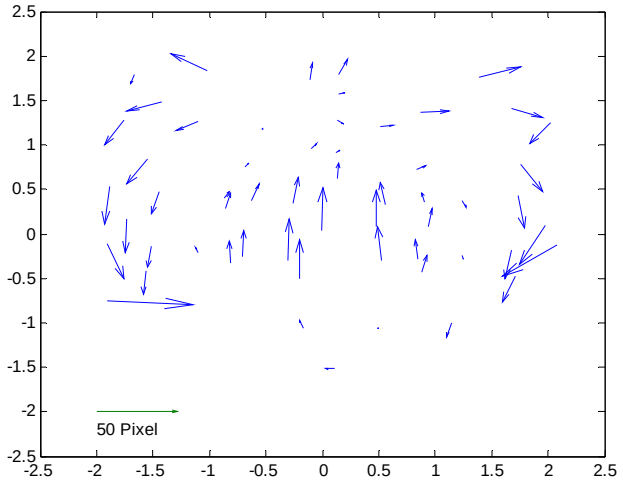

Figure 7. Residuals after the inclusion of Brown's parameters

Table 3. Comparison of parameter sets

set of parameters	s_0/mm
Grün	0.0005
Schut	0.0007
Mixed Model Brown	0.0011
Ebner	0.0017
Seidl	0.0033
Mauelshagen	0.0143
Kölbl	0.0151
El-Hakim	0.0466

In photogrammetric practice diverse sets of additional parameters have been developed, most of them intended for aerial photogrammetric applications. These sets of additional parameters can be classified into two types: the ones belonging to physically interpretable models and the ones belonging to mathematical models without physical interpretability, which are also termed rubber-parameters. The following list provides an overview of the sets of parameters used for our analysis: Mixed Model Brown [11], Ebner [12], Grün [13], Schut [14], Mauelshagen [15], Kölbl [16], El-Hakim [17], and Seidl [7]. All these sets were checked on their own as well as in combination with Brown's set for their applicability for the optical-power zoom objective. The combinations generated the best results (see Table 3). Figure 8 displays the corresponding residuals in extracts.

Following, we tried to extend the different combinations by the most significant parameters of other sets. However, we could no noticeably increase the accuracy (see Table 4).

Compared to the residual figure of the first feasible distortion model, the residual vectors of the photogrammetric sets of parameters are more randomly distributed. Nevertheless, small systematic errors remain. As shown in Table 3, the parameter set of Grün provides the highest accuracy ($s_0 = 0.0005$ mm). Transferred back to the object it results in a point accuracy of 0.3 mm at a distance of 3 m. However, the set of Grün consists of 44 parameters. A high number of parameters involves the risk of over-parameterization and may cause convergence problems.

An acceptable compromise between the number of parameters, the convergence, and the accuracy is the parameter set of Ebner. It contains 12 parameters, of which two can be eliminated, because they are already included in Brown's parameter set. The achievable accuracy of Ebner's set is $s_0 = 0.0017$ mm, which corresponds to a point accuracy of 1.1 mm at a distance of 3 m. It is recommended to continue using the parameter set of Ebner for further research.

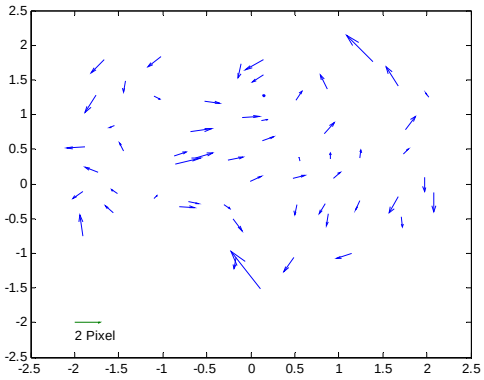

(a)

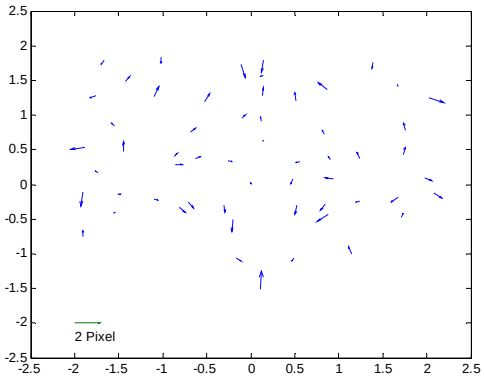

(b)

Figure 8. Residuals after the adjustment (a) Seidl, (b) Ebner, (c) Grün

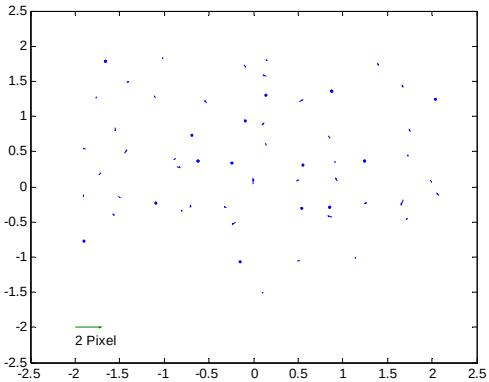

(c)

Table 4. Combination of the different parameter sets with significant parameters from other sets

set of parameters	s_0/mm
Grün	0.00054
Grün with El-Hakim	0.00050
Schut	0.00069
Schut with Kölbl	0.00065
Schut with El-Hakim	0.00066
Mixed Model Brown with ElHakim	0.00096

4. SUMMARY AND FUTURE WORK

More and more close-range and aerial photogrammetric applications demand for acquiring image data in the visual spectral range as well as the near- or mid-infrared spectral range at the same time. For the large field-of-view required in many photogrammetric applications, a four-mirror unobscured objective will be the favored approach. Because all-reflective objectives are free of chromatic aberrations, they can acquire image data in more than one spectral range simultaneously from the same position.

Based on an already realized OPZ setups we presented the first optical and opto-mechanical design for a full-frame dual-band unobscured objective, intended for high-resolution, close-range photogrammetric applications. Secondly, we described a monolithcal approach, which could be a very interesting solution in combination with UAVs. Due to the limited payload capacity of UAVs, the weight of the camera systems is of major importance. However, before the monolithcal approach can be realized, constraints, especially in the molding and ultra-precision manufacturing technology, have to be overcome.

To be able to use the full-frame dual-band unobscured objective as a close-range photogrammetric measurement system, a photogrammetric calibration has to be performed. Due to the similarity in the optical designs, photogrammetric calibration methods could be developed and tested on already existing OPZ demonstration systems. Existing distortion correction models for the OPZ based on optical simulation data were verified with photogrammetric methods and subsequently improved. After photogrammetric calibration, on could reach an accuracy of 1.1 mm in an object distance of 3 m with the OPZ system. In the future, the calibration method should be further improved and verified with the realized full-frame dual-band unobscured optical system.

ACKNOWLEDGEMENT

The authors would like to thank the German Research Foundation (DFG) for the financial support providing within the research project MA 2504/13-1.

REFERENCES

[1] K. Seidl, J. Knobbe, and H. Grüger, "Design of an all-reflective unobscured optical-power zoom objective", Applied Optics 48(21), 4097-4107 (2009).
[2] L. A. Ruiz, J. L. Lerma, and J. Gimeno, "Application of computer vision techniques to support in the restoration of historical buildings", Proc. of ISPRS Comission III Symposium 2002, Graz (2002).
[3] J. L. Lerma, L. A. Ruiz, and F. Buchon, "Application of spectral and textural classifications to recognize materials and damages on historic building facades", International Archives of Photogrammetry and Remote Sensing. Vol. XXXIII, Part B5, Amsterdam (2000).
[4] F. Rovira-Más, "Sensor Architecture and Task Classification for Agricultural Vehicles and Environments", Sensors 10, 11226-11247 (2010).
[5] http://www.flir.com/uploadedFiles/Eurasia/MMC/Appl_Stories/AS_0030_EN.pdf
[6] http://www.optosolutions.com/doc/Infrasil.pdf
[7] K. Seidl, J. Knobbe, D. Schneider, H. Lakner: „Distortion correction of all-reflective unobscured optical-power zoom objective", Applied Optics 49(14), 2712-2719 (2010).
[8] http://www.asctec.de/asctec-falcon-2/
[9] http://www.zeonex.com
[10] http://www.contrastoptical.com/Services/OpticalDesign/ImagingSystems/FreeformImaging/tabid/79/Default.aspx
[11] D. C. Brown, "The bundle adjustment - Progress and prospects", Proc. XIIIth Congress of the ISP, Commission III, (1976)
[12] H. Ebner, "Self-calibrating block adjustment", Proc. XIIIth Congress of the ISP, Commission III, (1976)
[13] A. Grün, "Experiences with the self-calibrating bundle adjustment", Proc. ACSM-ASP Convention, Washington, D.C. (1978)
[14] G. H. Schut, "Selection of additional parameters for bundle adjustments", Proc. Symposium of Commission III of the ISP, Moscow (1978)
[15] L. Mauelshagen, „Teilkalibrierung eines photogrammetrischen Systems mit variabler Passpunktanordnung und unterschiedlichen deterministischen Ansätzen", *DGK, Reihe C.,* Nr. 236 München (1977).
[16] J. Juhl, "Results from Jämijärvi", Contributions to the ISP WG III/3 Seminar, pp. 39–52 (1979).
[17] S. F. El-Hakim, and W. Faig, "Compensation of systematic image errors using spherical harmonica", Proc. of the American Society of Photogrammetry, Fall Technical Meeting, pp. 492–499 (1977).